No. 2310453122

2023年全国大学生英语竞赛(NECCS)

2023 National English Competition for College Students

获奖证书

CERTIFICATE OF AWARD

魏子祺 同学：

你在2023年全国大学生英语竞赛(NECCS)中，成绩优异，荣获 C 类三等奖。

特发此证，以示表彰。

You have obtained the ***Third Prize*** for Type C in 2023 National English Competition for College Students.

This certificate of commendation is hereby awarded to you as an encouragement.

国际英语外语教师协会

中国英语外语教师协会

二〇二三年六月二日

IATEFL · TEFL China

高等学校大学外语教学研究会

二〇二三年六月二日

College English Teaching & Research Association of China

共青团西北农林科技大学委员会

证　明

中国国际大学生创新大赛（2025）陕西赛区省级复赛已于7月结束，我校作品《满载“耳”归——新型黑木耳安全生产及高值化加工赋能乡村振兴》（团队成员：甄玉荷、宋金宜、王兴楠、王睿楠、张文超、高一炫、李世琦、李金宇、李心雨、魏子祺、李欣颜、刘悦、王赛群，指导教师：王周利）获得“青年红色筑梦之旅”赛道铜奖，获奖信息已在教育厅网站公示。

特此证明。

共青团西北农林科技大学委员会

2025年9月8日

CULSC 第八届全国大学生生命科学竞赛（创新创业类）

获奖证书

获奖项目： 基于脂质组学揭示不同干燥方式对花粉脂质氧化的影响及分子机制

获奖学生： 陈雨娴、王菊、王诗媛、魏子祺、崔若澜、潘晓妍

指导老师： 赵丽丽

获奖单位： 西北农林科技大学

获奖类型： 二等奖（创新组）

证 书 号： CULSC2023CXCY0824

全国大学生生命科学竞赛委员会

二〇二三年八月

CULSC第十届全国大学生生命科学竞赛（创新创业类）

获奖证书

获奖项目：不同形态纳米纤维素制备、表征及应用研究

获奖学生：魏子祺 石倩 田思雨 王雨桐 辛紫晴

指导老师：杜双奎

获奖单位：西北农林科技大学

获奖类型：三等奖

证书编号：CULSC2025CS0809

全国大学生生命科学竞赛委员会

二〇二五年七月

西北农林科技大学
NORTHWEST A&F UNIVERSITY

大学生创新创业训练计划项目

结题证书

魏子祺同学主持，王雨桐、石倩、田思雨同学参与的国家级项目“纳米纤维素基Pickering乳液稳定机制及应用研究”（No.202410712020）顺利结题，评审结果为优秀，指导教师为杜双奎，特此证明。

西北农林科技大学

教务处

二零二五年五月二十八日

Carbohydrate Polymers 342 (2024) 122419

Contents lists available at ScienceDirect

Carbohydrate Polymers

journal homepage: www.elsevier.com/locate/carbpol

Comparative analysis of millet bran nanocelluloses with various morphologies: Revealing differences in the formation mechanism and structure characteristics

Yulian Zhu [a], Ziqi Wei [a], Fang Jiang [a], Wenxuan Hu [a], Xiuzhu Yu [a], Shuang-kui Du [a,b,*]

[a] College of Food Science and Engineering, Northwest A&F University, 22 Xinong Road, Yangling, Shaanxi 712100, China
[b] Shaanxi Union Research Center of University and Enterprise for Grain Processing Technologies, Yangling, Shaanxi 712100, China

ARTICLE INFO

Keywords:
Millet bran
Nanocellulose
Formation mechanism
Structure analysis

ABSTRACT

To investigate the differences of nanocelluloses with various morphologies, ammonium persulphate (APS) oxidation, H_3PO_4 dissolution and regeneration, and ball milling combined with 1-butyl-3-methylimidazolium chloride ([BMIM]Cl) as a medium were applied to isolate cellulose nanocrystals (MCNCs), cellulose nanospheres (MCNSs) and cellulose fibrils (MCNFs) from millet bran. The structure, properties, and formation mechanism of three nanocelluloses were comparatively investigated by Fourier transform infrared spectroscopy, X-ray diffraction, thermogravimetric analysis, atomic force microscope, scanning electronic microscope, and emulsifying ability evaluation. MCNCs had needle-like structures due to the removal of amorphous regions, MCNFs appeared fibrous structures due to swelling and mechanical force, and MCNSs displayed spherical structures through self-assembly. MCNCs and MCNFs were confirmed to exhibit cellulose I structures with crystallinities of 61.24 % and 50.09 %, respectively. MCNSs showed the highest crystallinity of 68.41 % with a cellulose II structure. MCNFs and MCNSs exhibited higher initial decomposition temperatures, while MCNCs showed the highest residual mass. MCNFs suspension showed the highest apparent viscosity, while MCNSs suspension demonstrated superior dispersion. MCNSs-emulsion displayed the smallest droplet size, and MCNFs-emulsion exhibited the highest viscosity. This study reveals the formation mechanisms and relationship between morphologies and properties of three millet bran nanocelluloses, providing a theoretical basis for their application.

1. Introduction

With the increasing demand for renewable natural resources, cellulose, as the most abundant natural polymer on Earth, has garnered increased favor due to its biocompatibility, biodegradability, renewability, environmental friendliness, and nontoxicity (Dai et al., 2020). As the primary structural component of plant cell walls, cellulose can be isolated from various common sources such as plants (i.e., agricultural residues, wood-based biomass), aquatic organisms (i.e., algae, tunicates), and can also be obtained through bacterial biosynthesis (i.e., *Rhodobacter*, *Agrobacterium*, *Achromobacter*, and *Acetobacter xylinum*) (Ji & Wang, 2023; Muiruri et al., 2023; Rajinipriya et al., 2018). In recent years, cellulose has attracted growing attention in the food industry due to its outstanding biodegradability, biocompatibility, and low cost. Cellulose is composed of D-glucose units that are linearly β-1,4-linked. It possesses numerous hydroxy groups, facilitating the formation of strong hydrogen-bond networks between and within cellulose chains (García et al., 2016). To expand the range of cellulose applications, various chemical modifications such as acid hydrolysis, esterification, and etherification, as well as physical methods like grinding, extrusion, ultrasound, and homogenization have been utilized (Aziz et al., 2022; Zhou et al., 2022).

Recently, nanomaterials developed from natural biomacromolecules have attracted extensive interest. Cellulose is especially widely utilized in nanomaterial technology due to its enormous potential for structural modification (Ji et al., 2023). Nanocellulose can be classified into cellulose nanofibrils (CNFs), cellulose nanocrystals (CNCs), and cellulose nanospheres (CNSs) based on their morphologies, dimensions, and aspect ratios (length/diameter) (Kargarzadeh et al., 2017). CNFs are typically produced through mechanical delamination from native

* Corresponding author at: College of Food Science and Engineering, Northwest A & F University, 712100 Yangling, China.
E-mail address: dushuangkui@nwafu.edu.cn (S.-k. Du).

https://doi.org/10.1016/j.carbpol.2024.122419
Received 21 March 2024; Received in revised form 3 June 2024; Accepted 18 June 2024
Available online 21 June 2024

cellulose, exhibiting 20–50 nm diameters and 500–2000 nm lengths. The production of CNFs generally involves ultrasonication, milling, microfluidization, high-pressure homogenization, and freeze-disintegration methods, offering attractive properties such as biocompatibility and biodegradability due to their green preparation (Xu et al., 2022). CNCs display a needle-like structure and have geometrical dimensions ranging from 5 to 50 nm in diameter and 100 to 500 nm in length, synthesized using strong acid hydrolysis or oxidant to eliminate amorphous regions from the native cellulose, resulting in highly rigid and pure crystalline structures (Dai et al., 2020). CNSs, characterized by spherical morphologies, can be prepared using top-down methods like chemical treatment, mechanical disintegration, and enzymatic hydrolysis, or bottom-up method involving the dissolution and regeneration of cellulose, showing the crystalline type of cellulose II (Kargarzadeh et al., 2017). Given the diverse dimensions and morphologies of nanocelluloses, their properties and applications may vary significantly. CNFs are usually utilized to produce gas barriers in paper and polymers, CNCs are typically applied as reinforcement agents in packaging materials and biomedical industries, and CNSs are commonly used as Pickering emulsion stabilizers and as well as magnetoelectric material (Ji et al., 2023; Tian et al., 2022; Zhou et al., 2022). Currently, there have been some reports on the preparation, characterization, and application of different morphologies of nanocelluloses (Liu et al., 2023; Ni et al., 2021; Zhang et al., 2020). However, limited research has focused on nanocelluloses with various morphologies derived from the same native cellulose materials. Also, few comparative studies have been conducted on the relationship between their morphologies and application potential.

Millet, as an essential cereal crop, domesticated several thousand years ago in Africa and Asia, holds significant importance in the food industry due to its versatile applications and its inherent ability to withstand drought (Yang et al., 2022). Millet bran is the by-product of millet processing that makes up about 8 %–15 % (w/w) of millet, with an annual production of >500,000 tons in China. Millet bran is abundant in cellulose (>30 % w/w), proteins, starch, lipids, polyphenols, and peptides (Chen et al., 2024; Li et al., 2022). However, millet bran is currently randomly disposed of or utilized as a feed for livestock, thereby limiting its potential value and efficiency of utilization. Although some experts have focused on adding value to millet bran through bioactive compounds (protein, polyphenol, polysaccharides) extraction and solid-state fermentation (Wang et al., 2023), the relevant information about millet bran as an inexpensive and excellent source for cellulose and nanocellulose extraction is still lacking.

This study hypothesizes that millet bran can be a viable raw material for cellulose extraction, subsequently enabling the isolation of nanocelluloses with different morphologies. As far as we know, comprehensive research on the preparation, characterization, and comparison of various nanocelluloses from millet bran has yet to be documented in the existing literature. Thus, the primary objective of this study is to produce three nanocelluloses of different morphologies using various methods (i.e., APS oxidation, H_3PO_4 dissolution and regeneration, and balling milling combined with [BMIM]Cl as a medium), and the structure and properties of the obtained samples are also comparatively investigated and compared. This study aims to reveal the formation mechanisms of nanocelluloses with various morphologies and the relationship between their morphologies and properties, as well as provide a theoretical basis and detailed information for effectively utilizing millet by-product.

2. Materials and methods

2.1. Materials

The millet bran was provided by the Agricultural Technology Promotion Center of Shenmu in Yulin, China. Ionic liquid 1-butyl-3-methylimidazolium chloride ([BMIM]Cl), APS, and $NaClO_2$ were purchased from Macklin Reagent Co., Ltd. (Shanghai, China). H_3PO_4, HCl, and NaOH were purchased from Kelong Reagent Co., Ltd. (Chengdu, China). All other chemicals and solvents used in this work were of analytical grade.

2.2. Preparation of millet bran cellulose

The millet bran cellulose (MC) was isolated from millet bran using a previous method with some modifications (Xiao et al., 2019). The dried millet bran was pulverized and passed through an 80-mesh sieve. The ground millet bran was mixed with ethanol (1:20 w/v) at room temperature for 12 h to remove the lipid fraction and dried naturally. The dried sample was hydrolyzed by 0.6 % (w/v) α-amylase (4000 U/g) at a ratio of 1:20 (w/v) and stirred at 70 °C for 1 h to remove the starch. The precipitate was collected by centrifuging at 3500 rpm for 10 min and drying at 60 °C for 24 h. The dried precipitate was then treated with 5 % NaOH solution (at a ratio of 1:20 w/v) with continuous stirring at 70 °C for 4 h. After removing the supernatant by centrifuging at 3500 rpm for 10 min and washing with distilled water, the residue was treated with $NaClO_2$ solution (5 % w/v pH 3.8–4.0, adjusted by acetic acid) under mechanical stirring at 70 °C for 5 h. Subsequently, the residue was rewashed with distilled water until the filtrate turned neutral, followed by freeze-drying and pulverization to pass through a 100-mesh sieve to obtain MC for further use.

2.3. Preparation of millet bran nanocelluloses with different morphologies

2.3.1. Preparation of millet bran cellulose nanocrystals

The cellulose nanocrystals were prepared using the APS oxidation method (Zhang et al., 2020). MC was mixed with 1 mol/L APS solution at 1:100 w/v and stirred at 70 °C for 16 h. After the reaction, the mixture was cooled to room temperature and centrifugated at 12000 rpm for 10 min to remove the supernatant. The collected precipitate was resuspended with distilled water several times and centrifugated under certain conditions (7000 rpm 10 min). The supernatant from each centrifugation was collected and dialyzed until the pH reached neutral. Finally, the suspension was sonicated at 300 W for 30 min using a 22 kHz ultrasonic cell pulverizer (Ningbo Scientz Biotechnology Co., LTD) to disperse the sample. The obtained millet bran cellulose nanocrystals (MCNCs) were stored at 4 °C for further use, with some of the suspension freeze-dried for structural characterization.

2.3.2. Preparation of millet bran cellulose nanospheres

The cellulose nanospheres were prepared using a phosphoric acid dissolution and regeneration method with some modifications (Feng et al., 2022). MC was wetted with distilled water at a ratio of 1:3 w/v and then mixed with precooled H_3PO_4 (4 °C) at a ratio of 1:50 w/v. The mixture was stored at 4 °C for 24 h to swell the MC fully and then stirred at 50 °C for 6 h to hydrolyze the sample. After the incubation, distilled water was added five times, and the mixture was stored at 4 °C overnight to facilitate the regeneration of cellulose into cellulose nanospheres. Subsequently, the regenerated nanocellulose was collected by centrifuging at 10000 rpm for 10 min. The precipitate was washed with distilled water and dialyzed until the pH reached neutral. The obtained millet bran cellulose nanospheres (MCNSs) were stored at 4 °C for further use, and some of the suspension was freeze-dried for structural characterization.

2.3.3. Preparation of millet bran cellulose nanofibrils

The cellulose nanofibrils were prepared by ball milling (YXQM-2 L, Mitr, Changsha, China) combined with [BMIM]Cl as a medium, according to a reported study (Dai et al., 2021). The 2 g MC was mixed with 40 mL of 50 wt% [BMIM]Cl solution (dissolved in distilled water) in a ball mill jar equipped with 24 g zirconia balls (the diameter and mass ratio of zirconia balls were 3 mm and 6 g, 5 mm and 8 g, and 7 mm and 10 g, respectively). The ball milling was processed at room temperature at 240 rpm/min for 3 h. The obtained product was

centrifugated at 10000 rpm for 10 min after picking out the zirconia balls and then dialyzed until the pH reached neutral to remove the [BMIM]Cl solution. The obtained millet bran cellulose nanofibrils (MCNFs) were stored at 4 °C for further use, and some of the suspension was freeze-dried for structural characterization.

2.4. Morphology observation

2.4.1. Scanning electron microscope

Scanning electron microscopy (SEM, Nova Nano SEM-450, FEI America) was applied to observe the microstructure of samples at an accelerating voltage of 5 kV. The MC sample was directly attached to the sample stage using carbon tape. The nanocellulose suspensions (0.01 %) were dispersed with the ultrasonic oscillator (KQ-700DE, Kunshan, China) at 300 W for 10 min, loaded on silicon pellets, dried at an ambient temperature, and then attached to the sample stage using carbon tapes. Subsequently, the prepared samples were sprayed with gold by a gold sprayer (108auto, Ted Pella, Inc., USA) for 300 s to prevent charging (Liu et al., 2023; Ma et al., 2023). The images were observed and collected at 4000×, 60,000×, and 120,000×.

2.4.2. Transmission electron microscope

Transmission electron microscope (TEM, HT7800, Hitachi, Japan) was used to evaluate the morphology surface of nanocelluloses. According to the reported method by Xiao et al. (2019), the nanocellulose suspensions were fully dispersed using an ultrasonic oscillator at 300 W for 10 min. Subsequently, a drop of dispersed sample suspension was placed on a copper grid and stained with 0.25 % uranyl acetate solution. Subsequently, the sample was dried at room temperature overnight and observed at the acceleration voltage of 80 kV.

2.4.3. Atomic force microscopy

Atomic force microscopy (AFM, Multimode-8 Bruker, USA) was used to investigate the surface topography and roughness characteristics of nanocelluloses. According to the reported method by Feng et al. (2022), the nanocellulose suspensions (0.0001 %) were dispersed using the ultrasonic oscillator at 300 W for 10 min and dropped on a piece of freshly cleaved mica substrate before drying overnight at room temperature. The images were collected under tapping mode.

2.5. Structure characterization

2.5.1. Zeta potential and polydispersity index

The zeta potential and polydispersity index (PDI) of nanocellulose suspensions (3 mg/mL, diluted with distilled water) were measured according to a previous method using a laser particle size analyzer (ZEN3600, Malvern, England) (Ni et al., 2021). The suspensions were dispersed using the ultrasonic oscillator at 300 W for 10 min. All measurements were carried out three times at 25 °C.

2.5.2. Fourier transform infrared spectroscopy

In order to evaluate the functional groups of samples, a Fourier transform infrared spectrometer (FTIR, Nicolet iS10, Thermo Fisher Scientific, America) was employed to obtain the FTIR spectra. The samples were mixed with KBr at 1:100 (w/w) and pressed into tablets using a tablet press (NL-15 Nuoleixinda Co., Ltd., Tianjin, China). The spectra were collected within the wave numbers range of 400 to 4000 cm^{-1} for 16 scans at a resolution of 4 cm^{-1}. The FTIR spectra of samples were analyzed and presented by Origin 2018.

2.5.3. X-ray diffraction (XRD)

The crystalline structures of samples were measured on an X-ray diffractometer (D8 ADVANCE A25, Bruker, Germany). The detection was conducted at 40 kV and 40 mA within the diffraction angle (2θ) of 5–50° with a scanning step of 0.0196° and a scanning speed of 5.476°/min. The XRD measurements were performed in triplicate, and the crystallinity index (CrI) was calculated according to the Segal method (Peak height method) (Feng et al., 2022; Segal et al., 1959) from the original data:

$$CrI\% = \frac{100(I_{Max} - I_{Am})}{I_{Max}} \quad (1)$$

where I_{Max} is the highest of scattered intensity at the main peak of 22.4° (cellulose I) and 19.6° (cellulose II), and I_{Am} stands for the height of the minimum peak intensity for the amorphous region at $2\theta = 18°$. The XRD spectra of samples were analyzed using Jade 6.5, and presented by Origin 2018 after subtracting the background.

2.6. Thermal analysis

The thermal stabilities of the samples were analyzed using a thermal analyzer (STA 7200RV, HITACHI, Japan). The thermogravimetric analysis (TGA) and derivative thermogravimetric analysis (DTG) curves were recorded at a constant heating rate of 10 °C/min from 30 to 580 °C under an N_2 atmosphere (Xiao et al., 2019).

2.7. Surface wettability

To determine the surface wettability of samples, the water contact angles (WCA) of nanocellulose tablets were measured using a WCA analyzer (Chengdejinhe JY-PHb, China). The sample powers were compressed to cylindrical tablets (10 mm diameter, thickness 1 mm) using a tablet press (NL-15 Nuoleixinda Co., Ltd., Tianjin, China) at 10 W for 3 min. Deionized water (5 μL) was carefully dropped on the tablet by a high-precision injector, and the angle between the baseline of the droplet and the tangent line was calculated via ImageJ software to determine the WCA (Jiang et al., 2023).

2.8. Rheological measurements

The rheological properties of nanocellulose suspensions (1 % w/v) were analyzed utilizing a TA Instruments rheometer (TA Instruments, DHR-1, USA) equipped with a 20 mm cone plate geometry. The shear viscosity was measured at an increasing shear rate range of 0.01–100 s^{-1} (Shafiei-Sabet et al., 2014).

2.9. Emulsion capacity evaluation

2.9.1. Preparation of nanocelluloses based Pickering emulsions

The Pickering emulsions stabilized by nanocelluloses were prepared by mixing 10 mL of 1 % nanocellulose suspensions with 5 mL of medium chain triglycerides (MCT). The mixture was homogenized using a high-speed homogenizer (IKA T18 Ultra-Turrax, Staufen, Germany) at 10000 rpm for 3 min.

2.9.2. Characterization of nanocelluloses based Pickering emulsions

The droplets of obtained emulsions were observed with an optical microscope (Nikon, Ni —U, Japan). The TA Instruments rheometer with a 20 mm cone plate geometry was used to measure the rheological properties of the emulsions. The shear viscosity was measured at an increasing shear rate range of 0.1–100 s^{-1} (Jiang et al., 2023).

The laser particle size analyzers (Beckman Coulter LS13320, America; Malvern ZEN3600, England) were used to measure the particle size and zeta potential of the emulsions. In preparation for potential measurements, the emulsions were diluted by distilled water for 500 times and dispersed using the ultrasonic oscillator at 300 W for 10 min. The MCT solution was used as a control (Taha et al., 2018).

2.10. Statistical analysis

All experiments in this study were performed independently at least

three times. The obtained data was analyzed using SPSS 23.0, and the significant difference was determined by the one-way fixed-effects analysis of variance (ANOVA) test and Duncan's multi-range test.

3. Results and discussion

3.1. Mechanism for preparing millet bran nanocelluloses with different morphologies

Fig. 1 illustrates the schematic of different morphologies via the APS oxidation method, phosphoric acid regeneration method, and ball milling combined with [BMIM]Cl as a medium. The glucose molecules in native cellulose are tightly connected via β-1,4-D-glycosidic bonds to form cellulose chains and different cellulose chains are connected through hydrogen bonding and van der Waals forces to form microfiber chains, which then combined to form cellulose fibers (García et al., 2016). These hydrogen bond networks are firmly and tightly wrapped with cellulose fibers, forming a large agglomerated bundle structure. In order to produce nanocelluloses, nanotechnologies were adopted to disrupt the strong networks of inner native cellulose to release nanocellulose particles. Generally, different nanotechnologies are the main factors in forming nanocelluloses with various morphologies and properties. Hence, the hypotheses of the formation mechanism of nanocelluloses with various morphologies are based on the following principles.

In the preparation of MCNCs by APS oxidation, APS will decompose under heating conditions to produce sulfate radical anion ($SO_4^{\bullet -}$), hydrogen sulfate ion (HSO_4^-), and hydrogen peroxide (H_2O_2). These ions will destroy the β-1,4-D-glycosidic bonds in cellulose, attack the amorphous region of the cellulose, loosen the cellulose structure, and release the cellulose nanocrystals with small particle sizes. Meanwhile, the strong oxidation of hydrogen peroxide converts the C_6-OH groups of cellulose to -COOH groups (Liu et al., 2020; Ma et al., 2023), resulting in cellulose nanocrystals with carboxyl groups.

The polar hydroxyl groups in cellulose can strongly absorb the H_3PO_4 molecules with strong electronegativity. When the cellulose is mixed with phosphoric acid at a high concentration, the phosphoric acid molecules will diffuse into the crystalline and amorphous regions of the cellulose chains. Subsequently, the hydrogen bonds between the cellulose chains are replaced by those between the phosphoric acid molecules and the cellulose, and the contact network structure of the cellulose chains will be destroyed. Eventually, the phosphoric acid molecules will fill the space between cellulose chains, causing the cellulose to swell into a gel state. During hydrolysis at 50 °C, the gel-like dissolved cellulose is exposed to phosphoric acid and destroyed into molecular chains. As acid hydrolysis time rises, the cellulose molecular chains hydrolyzed by phosphoric acid gradually shorten, exposing more hydroxyl groups (Kassem et al., 2020; Kusmono & Affan, 2022; Su et al., 2022). Some short chains will form tiny aggregates once the intermolecular hydrogen bonding force rises. In the process of adding deionized water to regenerate the nanocellulose, many free molecular chains will form stable spherical structures on tiny aggregates through hydrophobic forces and hydrogen bonding. With the increase of acid hydrolysis time, the molecular chains of cellulose are destroyed more thoroughly, forming more short chains. Since the hydrogen bond content within and between cellulose molecular chains determines the crystallinity of cellulose, as the acid hydrolysis time increases, the hydrogen bonds between the molecular chains of regenerated cellulose strengthen, and the crystallinity of the cellulose nanospheres increases.

The ions of [BMIM]Cl solution (i.e., anion (chloride) and cation (1-butyl-3-methylimidazolium) will interact with the hydroxyl groups in the cellulose molecules, resulting in the breakage of the hydrogen bonds between the cellulose chains. The crystalline region of the cellulose molecule will be destroyed, and the amorphous part will swell as a result

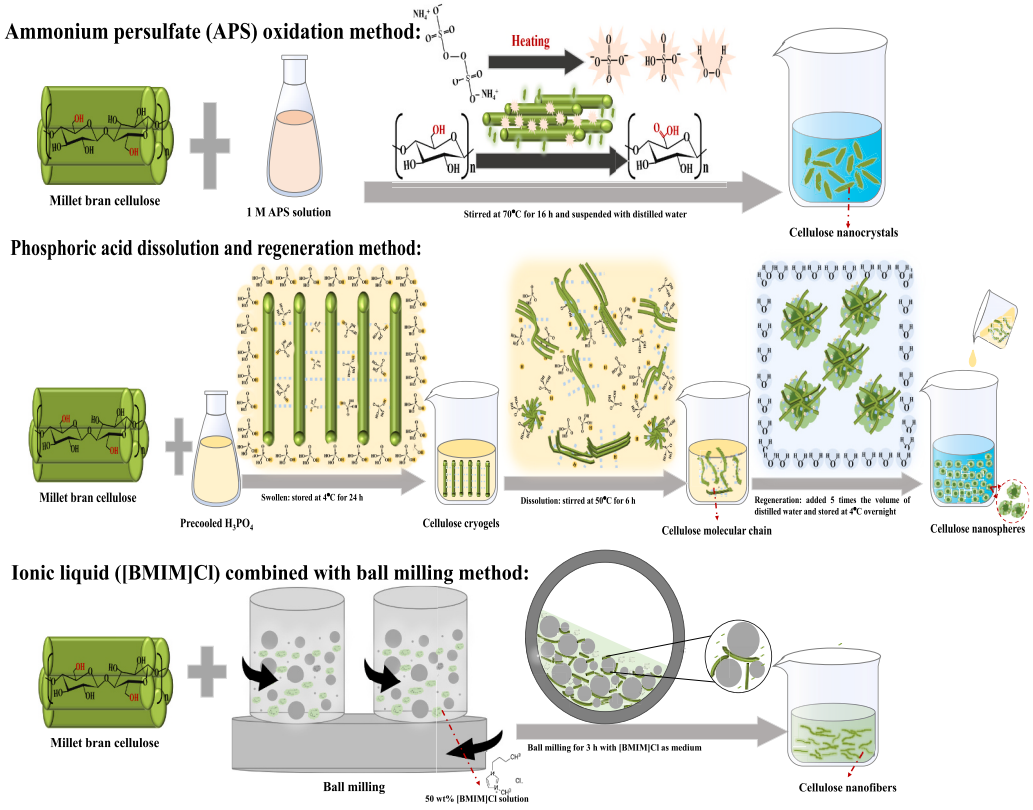

Fig. 1. Schematic diagram illustrating the preparation mechanism of nanocellulose with different morphologies via APS oxidation method, phosphoric acid regeneration method, and ball milling combined with [BMIM]Cl as a medium.

of the ionic liquid filling the space between the cellulose chains (Abdalla et al., 2022). After swelling, the compact structure of native cellulose will be destroyed, and the intact native fibers will become loose and wrinkled. Even if the ball milling is carried out at room temperature, friction between balls and between balls and tank walls will generate heat, which activates the interaction between [BMIM]Cl ions and cellulose hydroxyl groups, leading to hydroxyl group breakage in the different cellulose chains (Phanthong et al., 2017). The strong shear and friction forces produced by the ball milling process will also weaken the hydrogen bonds between the fibers, causing further disruption of the solubilized cellulose structure and releasing shorter nanofibrils. Moreover, due to the swelling of cellulose by ionic liquid, nanocellulose can be produced more efficiently during ball milling.

3.2. Morphology analysis and size distribution of millet bran cellulose and nanocelluloses

Fig. 2 presents the morphologies of MC, MCNCs, MCNFs, and MCNSs obtained by SEM, TEM, and AFM observations. The quantitative analysis of the length and diameter distributions of nanocelluloses obtained from SEM images is analyzed by ImageJ software and is exhibited in Fig. 2 and Table 1. The native MC exhibited a compact rod-like structure at the micron scale, demonstrating the removal of lignin and hemicellulose during pretreatment. Additionally, the micron size of MC may render it susceptible to chemical or physical disruption into nanoscale fibrils. The preparation process involves removing fat through ethanol soaking, followed by alkaline treatment to eliminate starch, protein, hemicellulose, and a portion of lignin. Subsequent bleaching treatment with sodium chlorite removes residual components, resulting in the final millet bran cellulose (Xiao et al., 2019). The three types of nanocelluloses show significant differences in morphology and size (Fig. 2A-C). MCNCs

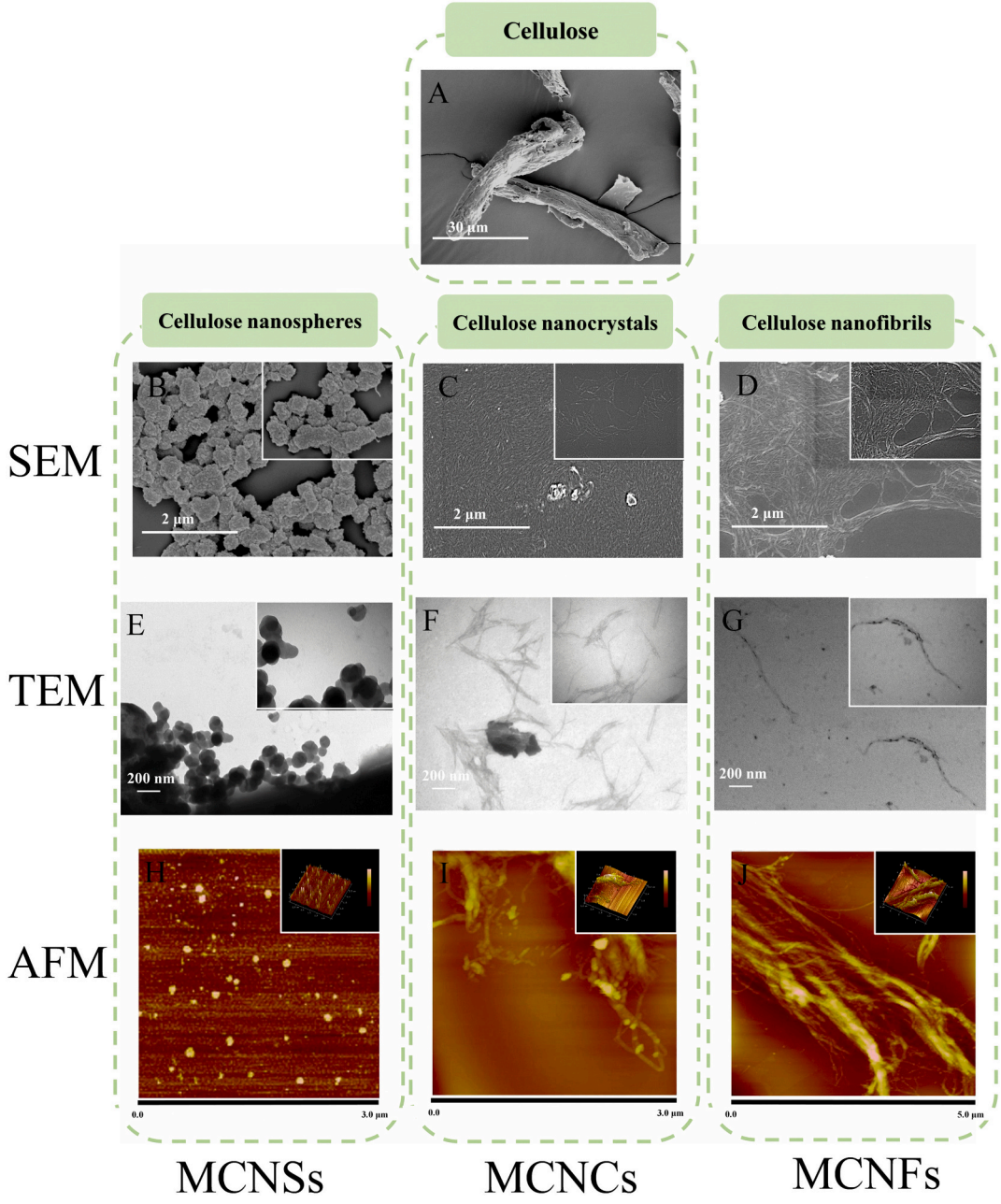

Fig. 2. Microscopy images of MC and nanocelluloses with different morphologies.

Table 1
The yield and average dimensions of nanocelluloses, and the crystallinity of MC and nanocelluloses.

Sample	Yield %	Length, L nm	Diameter, D nm	Aspect ratio, L/D	Crystallinity %	The mean size of emulsions μm
MC	–	–	–	–	52.68 ± 1.13c	
MCNCs	36.67 ± 2.90c	262.90 ± 31.14b	17.52 ± 0.97b	16.46 ± 1.97b	61.24 ± 2.55b	47.24 ± 0.54b
MCNSs	45.82 ± 3.12b	–	249.10 ± 33.50a	–	68.41 ± 0.78a	45.43 ± 3.50b
MCNFs	78.00 ± 0.55a	885.12 ± 195.81a	15.02 ± 1.56b	65.73 ± 12.32a	50.09 ± 3.21c	64.16 ± 1.93a

Data are mean ± standard deviations ($n = 3$), and the values followed by different letters in the same column indicate the significant difference ($P < 0.05$).

displayed a needle-like structure with an average length and diameter of approximately 262.90 nm and 17.52 nm, respectively. MCNSs presented a spherical structure with an average diameter of 249.10 nm. MCNFs exhibited a fibrous structure with an average length and diameter of approximately 885.12 nm and 15.02 nm, respectively (Table 1). The TEM observation displayed the spherical structure of MCNSs, the needle-like structure of MCNCs, and the fibrous structure of MCNF, all within the nanoscale range. These findings mostly agreed with the reported studies of nanocelluloses with different morphologies isolated from microcrystalline cellulose and Sunn hemp (Feng et al., 2022; Mahur et al., 2023), confirming the successful preparation of three millet bran nanocelluloses with various morphologies. According to the AFM results, the morphologies of nanocelluloses were elucidated in more depth through height sensor pictures and 3D images. The results of AFM also indicated that three nanocelluloses exhibit different morphologies, and their 3D structures were consistent with the observation of SEM. Three nanocelluloses differed from the 3D results, in which the spherical MCNSs showed uniformly distributed particles with better dispersion. In contrast, the needle-like MCNCs and elongated fibrous MCNFs displayed some aggregation. This indicated the presence of adhesion and entanglement behaviors between MCNCs and MCNFs particles, possibly attributed to their larger length in the structure (Mahur et al., 2023). Moreover, the varied morphologies of nanocelluloses were likely influenced by their preparation methods and formation mechanisms. The needle-like structure of MCNCs may be attributed to the elimination of amorphous regions from native cellulose by oxidation, the spherical structure of regenerated MCNSs may be due to the self-assembly of dissolved cellulose chains, and the fibrous structure of MCNFs may be caused by the high shear force exerted by ball milling equipment (Dai et al., 2021; Ma et al., 2023). The different morphologies and size distributions of MCNCs, MCNFs, and MCNFs (Fig. 3) may impart them with distinct properties.

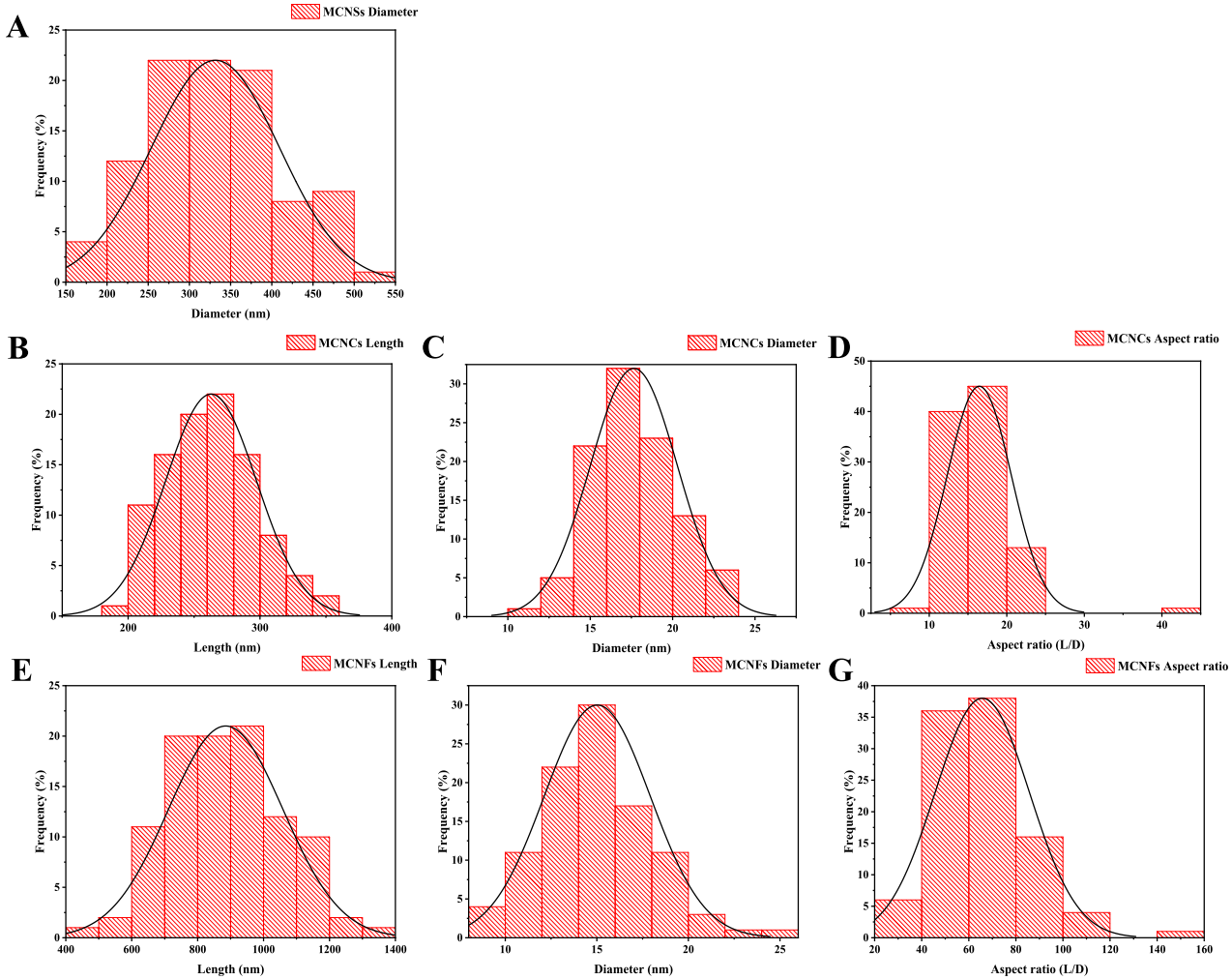

Fig. 3. Length, diameter, and aspect ratio of nanocelluloses.

3.3. Yield, zeta potential, and dispersity

The yields of MCNCs, MCNSs, and MCNFs are 36.67 %, 45.82 %, and 78.00 %, respectively (Table 1). The lowest yield of MCNCs may be attributed to the removal of amorphous regions during the APS oxidation and the discarding of large particles during the resuspension by distilled water for MCNC isolation (Ma et al., 2023). Fig. 4A and B present the zeta potential and PDI values of three nanocelluloses. MCNCs and MCNSs exhibited higher absolute zeta potential values of −38.93 mV and − 27.5 mV respectively, with the PDI of 0.77 and 0.16. MCNFs possessed the lowest zeta potential value of −23.53 mV with the highest PDI value of 1. The higher PDI values of MCNCs and MCNFs indicated the aggregation of samples, which may be attributed to their higher aspect ratios. Increased aspect ratios typically lead to heightened van der Waals forces, resulting in particle aggregation. This aggregation diminishes the exposure of hydroxyl groups to water, reducing electrostatic repulsion and zeta potential (Pawcenis et al., 2022). Zeta potential is a critical parameter indicating aggregation and stability of nanocellulose suspensions, reflecting the potential difference between the continuous phase and the stable fluid layer surrounding dispersed particles (Gao et al., 2023). Generally, larger absolute zeta potential values correspond to more excellent system stability, as significant charge repulsion between nanoparticles prevents aggregation, maintaining a uniform dispersion system (Tang et al., 2024). The three nanocelluloses in this study exhibit negative charges due to the inherent negative charge of cellulose and the introduction of negatively charged phosphate groups during phosphoric acid hydrolysis, sulfate groups during APS oxidation, and the swelling of [BMIM]Cl solution. MCNCs and MCNSs possessed higher absolute zeta potential values, attributed to the carboxyl groups introduced by APS oxidation and the introduction of phosphate groups ($-OPO_4^-$) via phosphoric acid hydrolysis (Liu et al., 2023; Ma et al., 2023).

3.4. FTIR analysis

The FTIR spectra of MC, MCNCs, MCNFs, and MCNSs are depicted in Fig. 5A. According to reported studies on cellulose and nanocelluloses, the peaks observed at 3400 and 2900 cm^{-1} corresponded to the characteristic peaks of the intra- and intermolecular hydroxyl group (-OH) and carbonyl group ($-CH_2$) (Zhang et al., 2020). Compared with MC, the intensity -OH absorption peak of the nanocelluloses around 3400 cm^{-1} increased (Fig. S1). Besides, the -OH absorption peak of MCNSs moved to the higher wavenumber significantly, indicating the strong red shift and suggesting the formation of more hydrogen bonds. This phenomenon may be attributed to the smaller particle size of nanocelluloses, exposing more -OH groups on the surface, which in turn interact to form intermolecular hydrogen bonds (Samsalee et al., 2023; Taheri et al., 2020). MCNCs had characteristic peaks at 1730 cm^{-1}, implying the oxidation of hydroxyl groups into carboxyl groups due to the APS oxidation (Ma et al., 2023). The peak at 1645 cm^{-1} was attributed to the O—H bending of absorbed water (Zhang et al., 2020). The absorption peak around 1379 cm^{-1} of samples was assigned to the vibrations of C—O and C—O exist in the polysaccharide rings of cellulose (El-Fattah et al., 2024). For the spectra of all samples, the bands around 1368 and 1318 cm^{-1} were mainly attributed to the parent chains of cellulose (Ebrahimi et al., 2024). The spectra of MCNSs showed split bands in the region of 1300–1210 cm^{-1} (circled in red), which were associated with the P═O stretching vibration (Liu et al., 2023). The peaks at 1163, 1110, and 1066 cm^{-1} were assigned to the stretching vibration peaks of the ether bond (C-O-C), which belong to the skeletal vibrations and functional groups of the cellulose glucose unit (Zhang et al., 2024). The band at 891 cm^{-1} was attributed to the stretching vibration peak of the C—H bond of the β-$_D$-glucopyranose units of cellulose. In addition, the small peak around 665 cm^{-1} implied the out-of-plane bending of C-O-H (Ebrahim et al., 2024). These two peaks existed in spectra, reflecting the inherent structural characteristic peaks of cellulose molecules.

3.5. XRD analysis

Among the four polymorphs of crystalline cellulose (cellulose I, cellulose II, cellulose III, and cellulose IV), cellulose I and cellulose II are the most common polymorphs of cellulose of interest. Cellulose I is always described as natural cellulose, since it is usually obtained from natural organisms. Cellulose I in plant fibers can be converted into cellulose II through processes of dissolution and regeneration (Emenike et al., 2023). These two crystalline celluloses are usually identified by different crystalline peaks according to XRD results (Hao et al., 2015; Liu et al., 2023). The XRD patterns of MC, MCNCs, MCNFs, and MCNSs are depicted in Fig. 5B. MC, MCNCs, and MCNFs exhibited similar diffraction patterns, displaying peaks at 2θ=16°, 22.4°, and 34.7°, corresponding to the (110), (200), and (004) plans of cellulose I, respectively (Zhang et al., 2020). Compared with MC, the diffraction peak intensity in MCNCs increased, while the peak intensity of MCNFs decreased, indicating alterations in crystallinity. Notably, MCNSs displayed distinct diffraction peaks 12.1°, 19.6° and 22.1°, corresponding to the ($1\bar{1}0$), (110), and (020) plans in cellulose II, respectively (Liu et al., 2023). These findings suggested that APS oxidation and ball milling combined with [BMIM]Cl as a medium preserved the cellulose I polymorph, while the phosphoric acid dissolution and regeneration method transformed MC from cellulose I to cellulose II. Similar results were also reported in

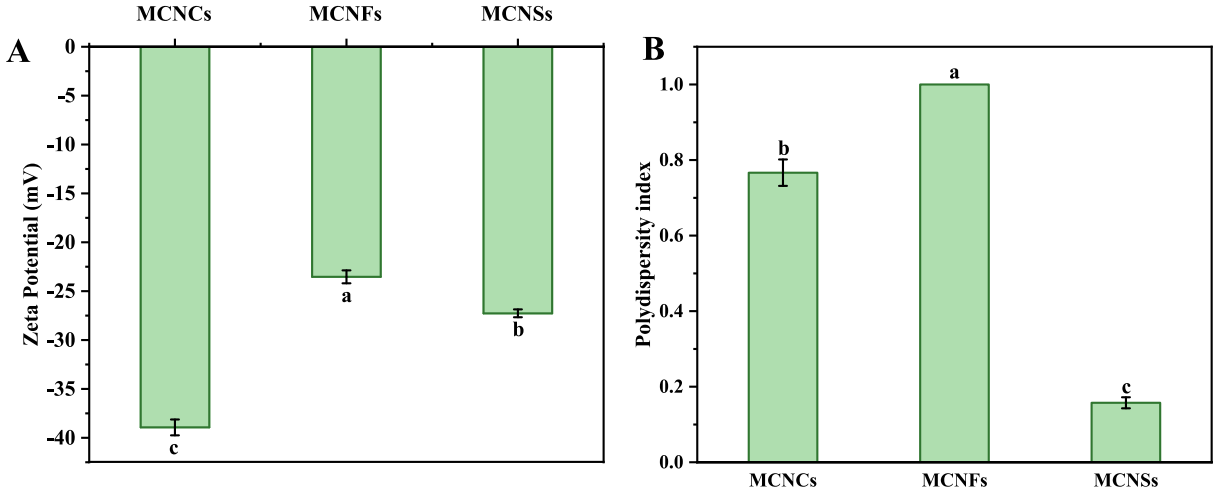

Fig. 4. Zeta potential (A) and polydispersity index (B) of nanocellulose suspensions.

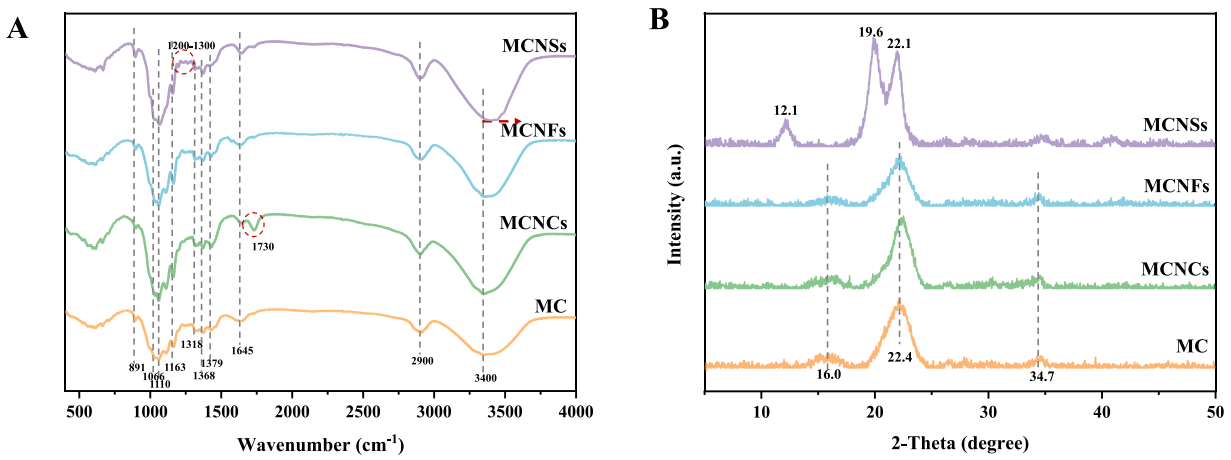

Fig. 5. FTIR spectrum (A) and XRD pattern (B) of native cellulose and nanocelluloses.

the cellulose nanocrystals isolated from litchi peels by APS oxidation and nanocellulose extracted from cellulose powder by ball milling with ionic liquid (Ma et al., 2023; Phanthong et al., 2017). The CI values of MC, MCNCs, and MCNFs are 52.68 %, 61.24 %, and 50.09 %, respectively (Table 1). The enhanced crystallinities of MCNCs may be attributed to the decomposition of amorphous regions in cellulose during APS oxidation, which leads to needle-like structures (Fig. 2) (Ma et al., 2023). Conversely, the decreased CI value of MCNFs may be due to the mechanical shear forces during ball milling, destroying both amorphous and crystalline regions. Additionally, the heat caused by ball milling increases the interaction between the anions and cations in [BMIM]Cl and the hydroxyl groups of cellulose, resulting in the breakage of hydroxyl groups in cellulose chains and the destruction of the crystalline region (Dai et al., 2021; Phanthong et al., 2017). It can be concluded that when ion liquid exists as a medium, it causes swelling in the amorphous region of cellulose and some crystalline regions. Compared with MC, MCNCs, and MCNFs, MCNSs exhibited higher crystallinity (68.41 %). The formation of MCNSs involves the initial dissolution of MC in phosphoric acid followed by regeneration with distilled water. This process disrupts the origin intermolecular hydrogen bonding network of cellulose and forms the regenerated cellulose nanospheres, which are commonly classified as cellulose II (Liu et al., 2023). In this study, the higher crystallinity of MCNSs was possibly due to the longer hydrolysis time adopted in the preparation. Hydrolysis time significantly influenced the structure and CI value of MCNSs, with a longer time leading to increased CI value (Fig. S2). During the dissolution of cellulose into phosphoric acid, the structure of cellulose is swollen and disrupted, and prolonged exposure to phosphoric acid results in the formation of smaller chains. In the subsequent regeneration process, more intermolecular hydrogen bonds will be formed and aggregated into samples with higher CI values (Tian et al., 2022).

3.6. Thermal analysis

As depicted in Fig. 6A, the thermogravimetric (TG) curves of all samples are similar and can be divided into three stages. The initial weight loss of samples occurs at around 120 °C, which can be attributed to the evaporation of water from samples. The second stage is 175–400 °C, where the sample mass begins to suffer a significant loss, ascribed to the thermal decomposition of cellulose itself. The mass loss at the range of 400–600 °C is due to the loss of the carbon-containing skeleton and leads to a mixture of carbon and hydrocarbons, and non-volatile components as residues (Xiao et al., 2019). The final char residues at 580 °C of MC, MCNCs, MCNSs, and MCNFs are 16.97 %, 25.92 %, 18.97 %, and 0.14 %, respectively. According to the derivative thermogravimetry (DTG) curves (Fig. 6B), the initial degradation temperatures of MC, MCNCs, MCNSs, and MCNFs are 231.41 °C, 200.59 °C, 242.22 °C, and 224.15 °C, respectively, with MCNCs exhibiting the lowest temperature. Similar results were also reported in another study, where the APS oxidated nanocelluloses with different pretreatments

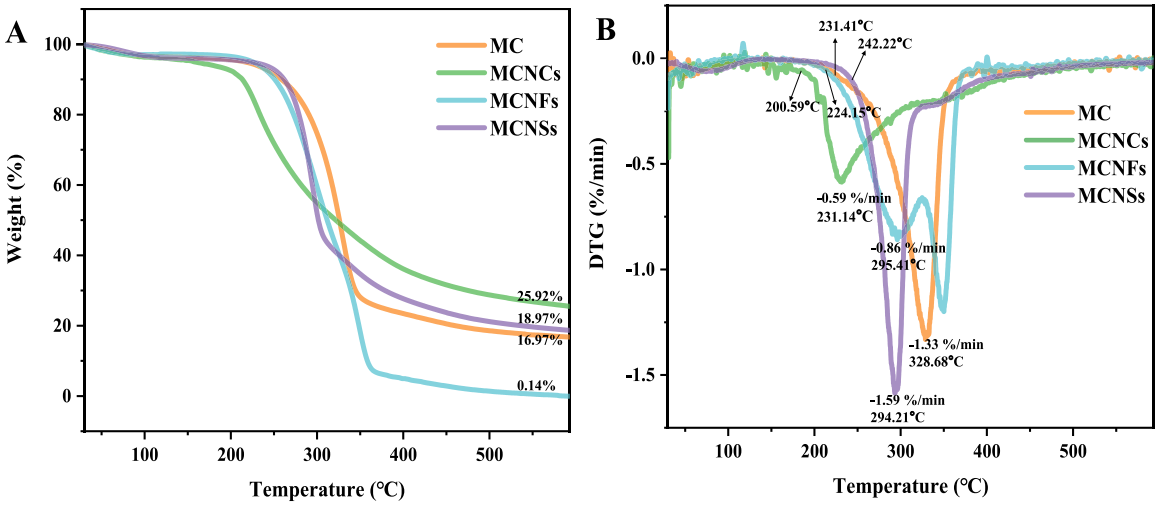

Fig. 6. TGA curves (A), and DTG curves (B) of native cellulose and nanocelluloses.

isolated from rice straw cellulose both exhibited an initial degradation temperature of around 250 °C, likely due to the increased heat transfer rates by the introduction of carboxyl groups (Oun & Rhim, 2018). Generally, surface carboxyl groups of MCNCs undergo a direct solid-to-gas phase transition during heating, which leads to a relatively lower initial degradation temperature (Jiang & Hsieh, 2013). The char residue of MCNCs was the highest, potentially due to the presence of carboxyl groups (as evidenced by the characteristic peak of carboxyl groups at 1730 cm^{-1} in the FTIR spectra of MCNCs in Fig. 5A). These groups will facilitate char residue formation at low temperatures, which may act as partial flame retardants (Cheng et al., 2014).

The DTG curves of MCNFs exhibited two peaks, possibly due to a portion of nanocellulose samples that have undergone ionic liquid swelling with a slightly loose structure that can be thermally degraded at a lower temperature (Phanthong et al., 2017). The higher maximum degradation temperature of MCNFs may be related to their aggregation into large bundle-like aggregates, which require a higher degradation temperature. Meanwhile, the lower initial degradation temperatures of MCNCs and MCNSs can be associated with their smaller particle sizes. The maximum thermal degradation rate of MCNSs was the largest, which may be related to their smallest particle size and larger exposure of the surface area to heat (Oun et al., 2018; Xiao et al., 2019). MCNSs can be thermally degraded more quickly when the degradation temperature was reached. Additionally, MCNSs exhibited a higher maximum degradation temperature at 294.21 °C, which may be related to their higher crystallinities, indicating a more stable structure. Generally, the thermal stability of polymers is closely correlated to their crystallinity, with higher crystallinity yielding better thermal stability (Chen et al., 2023). In summary, due to the larger particle size and higher crystallinity, MCNFs and MCNSs exhibited better thermal stabilities.

3.7. Surface wettability

The wettability of samples directly reflects the hydrophilicity or hydrophobicity of the particles. The surface wettability of solid particles is usually assessed using contact angle (θ). A lower contact angle indicates better wettability and hydrophilicity (Ebrahim et al., 2024). Fig. 7A presents the contact angles of MC, MCNCs, MCNFs, and MCNSs as 46.17°, 28.77°, 34.53°, and 27.07°, which are all <90°, revealing that the samples display hydrophilicity. Because of the reduction in particle size, the increase in specific surface area, and the enhanced exposure of hydroxyl groups, the contact angles of the nanocelluloses dropped, and their hydrophilicity enhanced when compared with native cellulose (Ni et al., 2021). Among the nanocelluloses, MCNFs exhibited the largest contact angle, followed by MCNCs, with MCNSs showing the smallest. Surface hydroxyl content and nonequivalent crystalline edges of cellulose structure (the (200) hydrophobic edge and (200) β / (220) α hydrophobic edge plane) are closely related to the contact angle of nanocellulose (Dai et al., 2020). The largest contact angle of MCNFs may be due to their longer fibrous structure, which makes it easier to aggregate and form larger aggregates with fewer exposed hydroxyl groups (Ni et al., 2021; Xu et al., 2022). As needle-shaped cellulose nanocrystals, MCNCs eliminate a portion of the amorphous region during APS oxidation while maintaining the hydrophobic edge surface (corresponding to the XRD results in Fig. 5B, where MCNCs showed a sharper diffraction peak at 22.9°), leading to a relatively higher contact angle (Dai et al., 2020). The contact angle of MCNCs here was higher than that of cellulose nanocrystals (25.91°) isolated from microcrystalline cellulose by sulfuric acid hydrolysis method (Wang et al., 2024), which may be due to the different preparation methods and the sources of cellulose materials. Due to the smallest particle size and distinct nanospherical structure of MCNSs, their larger specific surface area enabled them to expose more hydrogen bonds, exhibiting stronger hydrophilicity and a smaller contact angle. The regenerated cellulose is formed by self-assembly after fully dissolving the native cellulose and breaking the molecular chains. During the dissolution, the cellulose molecules are hydrolyzed into smaller molecular chains, forming numerous intermolecular hydrogen bonds (Liu et al., 2023; Tian et al., 2022). This result is consistent with the red-shifted -OH absorption peak of MCNSs in FTIR analysis (Fig. 5A).

3.8. Rheological properties of millet bran nanocellulose suspensions

Different types of nanocelluloses display varying viscosities within the same shear rate range (Fig. 7B). MCNFs exhibited the highest viscosity, followed by MCNCs, while MCNSs displayed the lowest viscosity. The different viscosities of three nanocellulose suspensions directly correlated with their morphologies and behavior during the stress application. MCNFs had the longest fibrous structure and the greatest aggregation, which may lead to the slowest molecular chain creep, contributing to their comparatively highest suspension viscosity. The longest fibrils can entangle each other to form a dense network structure that is least affected by shear stress and exhibits the highest viscosity (Padhi et al., 2023; Xu et al., 2022). Similar results are also reported in the study of Ni et al. (2021), where the nanocellulose suspension of ginkgo shell after high-pressure homogenization treatment also shows shear-thinning behavior in the rheological test. As the particle size of the nanocellulose increased, the viscosity increased proportionally with particle size. MCNSs possessed the smallest particles and were more likely to flow when shear stress was applied. Furthermore, due to the introduction of phosphate groups, MCNSs exhibited excellent dispersion, and it was difficult to form a three-dimensional network structure between molecules (Hao et al., 2015; Liu et al., 2023). Thus, the MCNSs suspension had the greatest fluidity and presented the relatively lowest viscosity. Despite their relatively smaller size, MCNCs exhibited slight

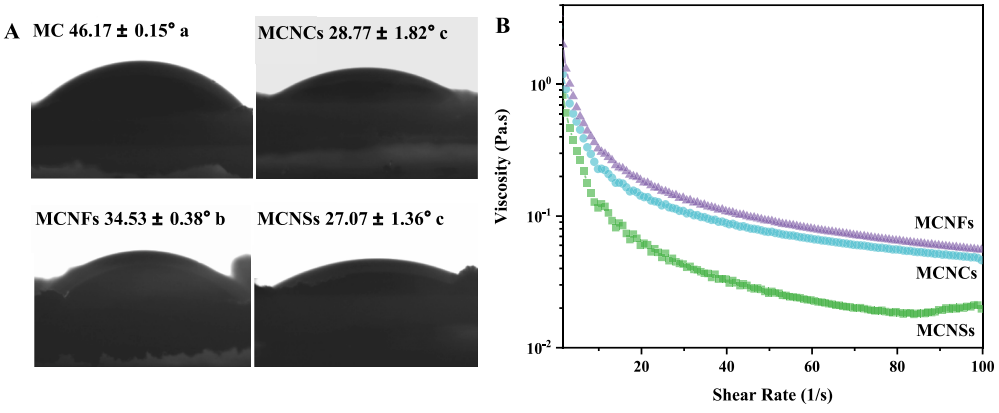

Fig. 7. (A) Contact angles of native cellulose and nanocelluloses; (B) Apparent viscosity of nanocellulose suspensions.

agglomeration between particles (Fig. 2), leading to a higher viscosity of MCNCs suspension. In summary, rheological studies revealed distinct behaviors for three nanocellulose suspensions, closely associated with their structures and morphologies. The varied rheological behaviors of the three nanocellulose suspensions and the viscosity change trends during shear stress application may directly affect their potential applications.

3.9. Characterization of emulsions stabilized by millet bran nanocelluloses

The particle size and stability of Pickering emulsions stabilized by nanocelluloses are usually closely correlated with the particle size and wettability of the stabilizers (Dai et al., 2020). Generally, improved dispersion, reduced wettability, and facile dispersion to the water-oil interface to form smaller and more stable emulsions are associated with nanocellulose particle size (Dai et al., 2020; Ji et al., 2023). As illustrated in Fig. 8D-F, the MCNSs-emulsion exhibited the particle size at a mean value of 45.43 μm, which was smaller than the MCNCs-emulsion (47.24 μm) and MCNFs-emulsion (69.07 μm). This conclusion was consistent with the emulsion microstructure observed in Fig. 8A-C. From the observation of emulsion microstructure, it can also be summarized that the droplet distribution in the MCNCs-emulsion was sparser than that of the MCNSs-emulsion, with some droplets exhibiting slight aggregation. Conversely, the MCNFs-emulsion exhibited only sparse droplets, predominantly with larger particle sizes. In addition, it can also be observed from Fig. 8C that some MCNFs particles were agglomerated into bundles (circled in red) filled in the continuous phase

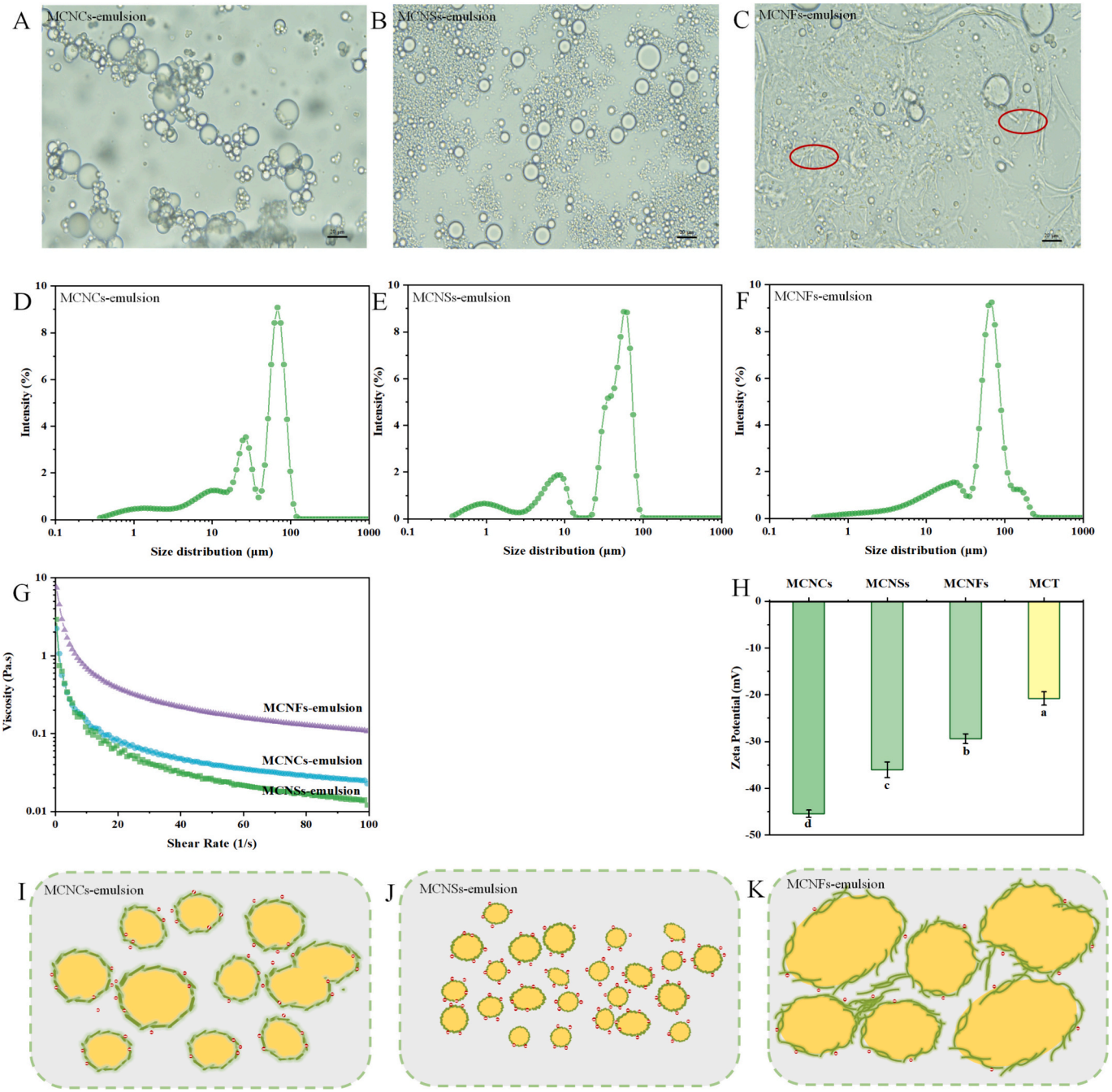

Fig. 8. Microscopic images (A-C), particle size distribution (D—F), apparent viscosity (G), zeta potential (H), and schematic diagram of potential mechanism (I—K) of different nanocelluloses stabilized emulsions.

of MCNFs-emulsions. This may be due to the larger particle size of MCNFs, which limited the dispersibility of some particles in the suspension at the water-oil interface during the preparation of emulsion (Ni et al., 2021), and therefore the number of the MCNFs-emulsion droplets observed was also less. Fig. 8G exhibits the apparent viscosity of emulsions stabilized by nanocelluloses with different morphologies. All of the nanocellulose-emulsions showed higher apparent viscosities at low shear stress, and the viscosities of emulsions decreased with increasing shear rate, showing a shear-thinning behavior. This indicated that the nanocellulose-based emulsions are non-Newtown fluids (Feng et al., 2023). Moreover, among the three emulsions, the MCNFs-emulsion showed the highest viscosity, followed by MCNCs-emulsions, and MCNSs displayed the lowest viscosity. The tendency was consistent with the viscosity of nanocellulose suspensions in Fig. 7B. The higher viscosity of MCNFs-emulsion may be directly related to the aggregated MCNFs particles filled in the continuous phase (Fig. 8C). The electrical surface potential of Pickering emulsion droplets is a critical factor that influences the stability of nanocellulose-based Pickering emulsions (Liu et al., 2024). Therefore, the zeta potentials of Pickering emulsions stabilized by three nanocelluloses with various morphologies were examined and presented in Fig. 8H. MCNCs-emulsion and MCNSs-emulsion were endowed with higher absolute values of zeta potential, which may be related to more surface charge groups introduced by MCNCs and MCNSs. The higher absolute zeta potential values of these two emulsions may also lead to more dispersed droplets since greater surface potential on the emulsion droplets will generate stronger repulsive forces to prevent droplets from aggregating (Taha et al., 2018).

The morphology of nanocelluloses may directly influence their emulsification ability (Kalashnikova et al., 2013; Li et al., 2018). MCNSs exhibited the smallest particle size, higher charge density, and optimal dispersion characteristics. Consequently, MCNSs can rapidly disperse to the water-oil interface during emulsification, forming smaller droplets. As for MCNCs, although they showed a slight agglomeration tendency, their relatively smaller size was beneficial for stabilizing emulsion (Dai et al., 2020). However, due to the relatively longer size and lowest charge density, MCNFs exhibited higher intermolecular viscosity (Fig. 7B). The entanglement of MCNFs molecules endowed them with lower surface coverage, which was insufficient to form a viscoelastic interface barrier to protect emulsion against coalescence (Ni et al., 2021). Moreover, although some MCNFs particles can disperse to the surface of emulsion droplets, their tendency to aggregate, entangle, and exhibited lower spatial resistivity led to the formation of larger droplets. This conclusion was in agreement with the previous studies (Kalashnikova et al., 2013; Ni et al., 2021), in which longer nanocellulose caused lower surface coverage and formed larger emulsion droplets, while nanocellulose in smaller size resulted in smaller emulsion droplets and better emulsification ability.

4. Conclusion

Different morphologies of nanocelluloses (MCNCs, MCNFs, and MCNSs) were successfully prepared using APS oxidation, H_3PO_4 dissolution and regeneration, and ball milling combined with [BMIM]Cl as a medium. MCNCs and MCNFs exhibited the morphologies of needle-like structures, and typical fibrous structures belonged to cellulose I, while the MCNSs displayed a spherical structure and crystalline transformation to cellulose II due to the dissolution and regeneration processes. MCNSs and MCNFs exhibited better thermal stabilities due to the higher crystallinity and larger particle size. MCNFs tended to agglomerate, resulting in the highest apparent viscosity. MCNSs exhibited the best dispersion and greatest fluidity, facilitating their particles to rapidly disperse to the water-oil interface, forming droplets with the smallest particle size. While MCNFs-emulsion displayed the largest particle size and highest viscosity with aggregated MCNFs filled in the continuous phase. Overall, this study presents an approach to fabricating different morphologies of nanocelluloses from millet bran. Furthermore, the potential of nanocellulose utilized as a Pickering emulsion stabilizer has been primarily proposed. Subsequent studies can focus on improving the emulsifying capacity of nanocelluloses and investigate their specific emulsion stability mechanism to expand the applications in various fields.

CRediT authorship contribution statement

Yulian Zhu: Writing – original draft, Software, Methodology, Investigation. **Ziqi Wei:** Investigation, Data curation. **Fang Jiang:** Writing – review & editing, Conceptualization. **Wenxuan Hu:** Visualization, Software. **Xiuzhu Yu:** Writing – review & editing, Supervision, Conceptualization. **Shuang-kui Du:** Writing – review & editing, Resources, Funding acquisition, Conceptualization.

Declaration of competing interest

The authors declare that they have no personal or financial relationship with any individuals or organizations that could have appeared to influence the work reported in this paper.

Data availability

Data will be made available on request.

Acknowledgments

The authors would like to thank the Shaanxi Province Key Research and Development Program Project (2021NY-155), and National College Students' Innovation and Entrepreneurship Training Program (202401160AC) for the support.

Appendix A. Supplementary data

Supplementary data to this article can be found online at https://doi.org/10.1016/j.carbpol.2024.122419.

References

Abdalla, S. H., .G., Mahmood, H., Hilmi Bin Noh, M., & Moniruzzaman, M. (2022). Ionic liquid assisted nanocellulose production from microcrystalline cellulose: Correlation between cellulose solubility and nanocellulose yield via COSMO-RS prediction. *Journal of Molecular Liquids, 368*, Article 120591.

Aziz, T., Farid, A., Haq, F., Kiran, M., Ullah, A., Zhang, K., … Al Jaouni, S. K. (2022). A review on the modification of cellulose and its applications. *Polymers, 14*.

Chen, C., Yin, J., Jing, P., & Jiao, S. (2024). Effects of hot air-assisted radio frequency stabilization of brown millet and millet bran: Enzyme inactivation, microstructure, nutritional quality, and storage stability. *Innovative Food Science & Emerging Technologies, 91*, Article 103529.

Chen, Z., Xie, Z., & Jiang, H. (2023). Extraction of the cellulose nanocrystals via ammonium persulfate oxidation of beaten cellulose fibers. *Carbohydrate Polymers, 318*, Article 121129.

Cheng, M., Qin, Z., Liu, Y., Qin, Y., Li, T., Chen, L., & Zhu, M. (2014). Efficient extraction of carboxylated spherical cellulose nanocrystals with narrow distribution through hydrolysis of lyocell fibers by using ammonium persulfate as an oxidant. *Journal of Materials Chemistry A, 2*(1), 251–258.

Dai, H., Wu, J., Zhang, H., Chen, Y., Ma, L., Huang, H., Huang, Y., & Zhang, Y. (2020). Recent advances on cellulose nanocrystals for Pickering emulsions: Development and challenge. *Trends in Food Science & Technology, 102*, 16–29.

Dai, H., Zhang, H., Chen, Y., Ma, L., Wu, J., & Zhang, Y. (2021). Co-stabilization and properties regulation of Pickering emulsions by cellulose nanocrystals and nanofibrils from lemon seeds. *Food Hydrocolloids, 120*, Article 106884.

Ebrahimi, R., Fathi, M., & Ghoddusi, H. B. (2024). Pickering emulsions stabilized by cellulose nanocrystals extracted from hazelnut shells: Production and stability under different harsh conditions. *International Journal of Biological Macromolecules, 258*, Article 128982.

El-Fattah, W. A., Guesmi, A., Ben Hamadi, N., El-Desouky, M. G., & Shahat, A. (2024). A green synthesis of cellulose nanocrystals biosorbent for remediation of wastewater containing industrial dye. *Colloids and Surfaces A: Physicochemical and Engineering Aspects, 681*, Article 132729.

Emenike, E. C., Iwuozor, K. O., Saliu, O. D., Ramontja, J., & Adeniyi, A. G. (2023). Advances in the extraction, classification, modification, emerging and advanced applications of crystalline cellulose: A review. *Carbohydrate Polymer Technologies and Applications, 6*, Article 100337.

Feng, X., Dai, H., Fu, Y., Yu, Y., Zhu, H., Wang, H., Chen, H., Ma, L., & Zhang, Y. (2022). Regulation mechanism of nanocellulose with different morphologies on the properties of low-oil gelatin emulsions: Interfacial adsorption or network formation? *Food Hydrocolloids, 133*, Article 107960.

Feng, X., Dai, H., Tan, H., Tang, M., Ma, L., & Zhang, Y. (2023). Improvement of low-oil gelatin emulsions performance by adjusting the electrostatic interaction between gelatin and nanocellulose with different morphologies. *Food Hydrocolloids, 139*, Article 108592.

Gao, J., Qiu, Y., Chen, F., Zhang, L., Wei, W., An, X., & Zhu, Q. (2023). Pomelo peel derived nanocellulose as Pickering stabilizers: Fabrication of Pickering emulsions and their potential as sustained-release delivery systems for lycopene. *Food Chemistry, 415*, Article 135742.

García, A., Gandini, A., Labidi, J., Belgacem, N., & Bras, J. (2016). Industrial and crop wastes: A new source for nanocellulose biorefinery. *Industrial Crops and Products, 93*, 26–38.

Hao, X., Shen, W., Chen, Z., Zhu, J., Feng, L., Wu, Z., Wang, P., Zeng, X., & Wu, T. (2015). Self-assembled nanostructured cellulose prepared by a dissolution and regeneration process using phosphoric acid as a solvent. *Carbohydrate Polymers, 123*, 297–304.

Ji, C., & Wang, Y. (2023). Nanocellulose-stabilized Pickering emulsions: Fabrication, stabilization, and food applications. *Advances in Colloid and Interface Science, 318*, Article 102970.

Ji, Q., Zhou, C., Li, Z., Boateng, I. D., & Liu, X. (2023). Is nanocellulose a good substitute for non-renewable raw materials? A comprehensive review of the state of the art, preparations, and industrial applications. *Industrial Crops and Products, 202*, Article 117093.

Jiang, F., & Hsieh, Y.-L. (2013). Chemically and mechanically isolated nanocellulose and their self-assembled structures. *Carbohydrate Polymers, 95*(1), 32–40.

Jiang, F., Zhu, Y., Hu, W.-X., Li, M., Liu, Y., Feng, J., Lv, X., Yu, X., & Du, S.-k. (2023). Characterization of quinoa starch nanoparticles as a stabilizer for oil in water Pickering emulsion. *Food Chemistry, 427*, Article 136697.

Kalashnikova, I., Bizot, H., Bertoncini, P., Cathala, B., & Capron, I. (2013). Cellulosic nanorods of various aspect ratios for oil in water Pickering emulsions. *Soft Matter, 9*(3), 952–959.

Kargarzadeh, H., Ioelovich, M., Ahmad, I., Thomas, S., & Dufresne, A. (2017). Methods for extraction of nanocellulose from various sources. In *Handbook of nanocellulose and cellulose nanocomposites* (pp. 1–49).

Kassem, I., Kassab, Z., Khouloud, M., Sehaqui, H., Bouhfid, R., Jacquemin, J., … El Achaby, M. (2020). Phosphoric acid-mediated green preparation of regenerated cellulose spheres and their use for all-cellulose cross-linked superabsorbent hydrogels. *International Journal of Biological Macromolecules, 162*, 136–149.

Kusmono, & Affan, M. N. (2022). Isolation and characterization of nanocrystalline cellulose from ramie fibers via phosphoric acid hydrolysis. *Journal of Natural Fibers, 19*(7), 2744–2755.

Li, M., Chang, L., Ren, J., Jiang, F., Zhao, N., Liu, Y., Yu, X., & Du, S.-k. (2022). Nutritional, physical, functional properties and antioxidant potential of different colors proso millet husks and brans. *LWT, 171*, Article 114092.

Li, X., Li, J., Gong, J., Kuang, Y., Mo, L., & Song, T. (2018). Cellulose nanocrystals (CNCs) with different crystalline allomorph for oil in water Pickering emulsions. *Carbohydrate Polymers, 183*, 303–310.

Liu, B., Li, Y., Yuan, Y., Zheng, B., Liu, C., Zhou, L., & Zhang, J. (2023). Controllable self-assembly of cellulose nanospheres through phosphoric acid triggered dissolution-regeneration and degradation. *International Journal of Biological Macromolecules, 243*, Article 125119.

Liu, Y., Liu, L., Li, X., Yu, J., Chen, M., Lin, L., Jia, R., & Fan, Y. (2024). Pickering emulsions by combining nanocellulose/nanochitin and silk fibroin: Silk fibroin as a stabilizer or an emulsifier. *Industrial Crops and Products, 211*, Article 118270.

Liu, Y., Liu, L., Wang, K., Zhang, H., Yuan, Y., Wei, H., Wang, X., Duan, Y., Zhou, L., & Zhang, J. (2020). Modified ammonium persulfate oxidations for efficient preparation of carboxylated cellulose nanocrystals. *Carbohydrate Polymers, 229*, Article 115572.

Ma, Q., Nie, C., Bu, X., Liu, B., Li, W., Zhang, X., Tan, Y., Wu, P., Fan, G., & Wang, J. (2023). Properties of Pickering emulsions stabilized by cellulose nanocrystals extracted from litchi peels. *International Journal of Biological Macromolecules, 242*, Article 124879.

Mahur, B. K., Ahuja, A., Singh, S., Maji, P. K., & Rastogi, V. K. (2023). Different nanocellulose morphologies (cellulose nanofibers, nanocrystals and nanospheres) extracted from Sunn hemp (*Crotalaria Juncea*). *International Journal of Biological Macromolecules, 253*, Article 126657.

Muiruri, J. K., Yeo, J. C. C., Zhu, Q., Ye, E., Loh, X. J., & Li, Z. (2023). Bacterial cellulose: Recent advances in biosynthesis, functionalization strategies and emerging applications. *European Polymer Journal, 199*, Article 112446.

Ni, Y., Li, J., & Fan, L. (2021). Effects of ultrasonic conditions on the interfacial property and emulsifying property of cellulose nanoparticles from ginkgo seed shells. *Ultrasonics Sonochemistry, 70*, Article 105335.

Oun, A. A., & Rhim, J.-W. (2018). Isolation of oxidized nanocellulose from rice straw using the ammonium persulfate method. *Cellulose, 25*(4), 2143–2149.

Padhi, S., Singh, A., & Routray, W. (2023). Oscillatory and rotational rheological characterization of jackfruit peel cellulose suspension: Effect of concentration, pH and ionic strength. *Food Hydrocolloids, 145*, Article 109179.

Pawcenis, D., Leśniak, M., Szumera, M., Sitarz, M., & Profic-Paczkowska, J. (2022). Effect of hydrolysis time, pH and surfactant type on stability of hydrochloric acid hydrolyzed nanocellulose. *International Journal of Biological Macromolecules, 222*, 1996–2005.

Phanthong, P., Karnjanakom, S., Reubroycharoen, P., Hao, X., Abudula, A., & Guan, G. (2017). A facile one-step way for extraction of nanocellulose with high yield by ball milling with ionic liquid. *Cellulose, 24*(5), 2083–2093.

Rajinipriya, M., Nagalakshmaiah, M., Robert, M., & Elkoun, S. (2018). Importance of agricultural and industrial waste in the field of nanocellulose and recent industrial developments of wood based nanocellulose: A review. *ACS Sustainable Chemistry & Engineering, 6*(3), 2807–2828.

Samsalee, N., Meerasri, J., & Sothornvit, R. (2023). Rice husk nanocellulose: Extraction by high-pressure homogenization, chemical treatments and characterization. *Carbohydrate Polymer Technologies and Applications, 6*, Article 100353.

Segal, L., Creely, J., Martin, A. E. J., & Conrad, C. (1959). An empirical method for estimating the degree of crystallinity of native cellulose using the X-ray diffractometer. *Textile Research Journal, 29*, 786–794.

Shafiei-Sabet, S., Hamad, W. Y., & Hatzikiriakos, S. G. (2014). Ionic strength effects on the microstructure and shear rheology of cellulose nanocrystal suspensions. *Cellulose, 21*(5), 3347–3359.

Su, H., Wang, B., Sun, Z., Wang, S., Feng, X., Mao, Z., & Sui, X. (2022). High-tensile regenerated cellulose films enabled by unexpected enhancement of cellulose dissolution in cryogenic aqueous phosphoric acid. *Carbohydrate Polymers, 277*, Article 118878.

Taha, A., Hu, T., Zhang, Z., Bakry, A. M., Khalifa, I., Pan, S., & Hu, H. (2018). Effect of different oils and ultrasound emulsification conditions on the physicochemical properties of emulsions stabilized by soy protein isolate. *Ultrasonics Sonochemistry, 49*, 283–293.

Taheri, P., Jahanmardi, R., Koosha, M., & Abdi, S. (2020). Physical, mechanical and wound healing properties of chitosan/gelatin blend films containing tannic acid and/or bacterial nanocellulose. *International Journal of Biological Macromolecules, 154*, 421–432.

Tang, L., Wang, B., Bai, S., Fan, B., Zhang, L., & Wang, F. (2024). Preparation and characterization of cellulose nanocrystals with high stability from okara by green solvent pretreatment assisted TEMPO oxidation. *Carbohydrate Polymers, 324*, Article 121485.

Tian, W., Gao, X., Zhang, J., Yu, J., & Zhang, J. (2022). Cellulose nanosphere: Preparation and applications of the novel nanocellulose. *Carbohydrate Polymers, 277*, Article 118863.

Wang, Y., Huang, Y., Li, H., Luo, Y., Dai, D., Zhang, Y., Wang, H., Chen, H., Wu, J., & Dai, H. (2024). Low gelatin concentration assisted cellulose nanocrystals stabilized high internal phase emulsion: The key role of interaction. *Carbohydrate Polymers, 337*, Article 122175.

Wang, Z., Tang, H., Liu, G., Gong, H., Li, Y., Chen, Y., & Yang, Y. (2023). Compound probiotics producing cellulase could replace cellulase preparations during solid-state fermentation of millet bran. *Bioresource Technology, 385*, Article 129457.

Xiao, Y., Liu, Y., Wang, X., Li, M., Lei, H., & Xu, H. (2019). Cellulose nanocrystals prepared from wheat bran: Characterization and cytotoxicity assessment. *International Journal of Biological Macromolecules, 140*, 225–233.

Xu, Y., Xu, Y., Chen, H., Gao, M., Yue, X., & Ni, Y. (2022). Redispersion of dried plant nanocellulose: A review. *Carbohydrate Polymers, 294*, Article 119830.

Yang, T., Ma, S., Liu, J., Sun, B., & Wang, X. (2022). Influences of four processing methods on main nutritional components of foxtail millet: A review. *Grain & Oil Science and Technology, 5*(3), 156–165.

Zhang, H., Chen, Y., Wang, S., Ma, L., Yu, Y., Dai, H., & Zhang, Y. (2020). Extraction and comparison of cellulose nanocrystals from lemon (*Citrus limon*) seeds using sulfuric acid hydrolysis and oxidation methods. *Carbohydrate Polymers, 238*, Article 116180.

Zhang, X., Xi, C., Guo, S., Yan, M., Lu, Y., Sun, Z., … Li, W. (2024). Electron beam pre-irradiation enhances substitution degree, and physicochemical and functional properties of carboxymethyl peanut shell nanocellulose. *Industrial Crops and Products, 209*, Article 118035.

Zhou, L., Zhang, W., & Wang, J. (2022). Recent advances in the study of modified cellulose in meat products: Modification method of cellulose, meat quality improvement and safety concern. *Trends in Food Science & Technology, 122*, 140–156.